Case Study of an Intense African Easterly Wave

GARETH J. BERRY AND CHRIS THORNCROFT

Department of Earth and Atmospheric Sciences, The University at Albany, State University of New York, Albany, New York

(Manuscript received 1 June 2004, in final form 8 September 2004)

ABSTRACT

The life cycle of an intense African easterly wave (AEW) over the African continent is examined using European Centre for Medium-Range Weather Forecasts (ECMWF) operational analyses, Meteosat satellite images, and synoptic observations. This system, the strongest AEW of 2000, can be tracked from central North Africa into the eastern Atlantic Ocean, where it is associated with the genesis of Hurricane Alberto. Synoptic analysis of the kinematic and thermodynamic fields is supplemented by analysis of potential vorticity (PV), allowing exploration at the role of multiple scales in the evolution of this AEW.

The authors' analysis promotes the division of the AEW life cycle into three distinctive phases. (i) Initiation: The AEW development is preceded by a large convective event composed of several mesoscale convective systems over elevated terrain in Sudan. This convection provides a forcing on the baroclinically and barotropically unstable state that exists over tropical North Africa. (ii) Baroclinic growth: A low-level warm anomaly, generated close to the initial convection, interacts with a midtropospheric strip of high PV that exists on the cyclonic shear side of the African easterly jet, which is consistent with baroclinic growth. This interaction is reinforced by the generation of subsynoptic-scale PV anomalies by deep convection that is embedded within the baroclinic AEW structure. (iii) West coast development: Near the West African coast, the baroclinic structure weakens, but convection is maintained. The midtropospheric PV anomalies embedded within the AEW merge with one another and with PV anomalies that are generated by convection over topography ahead of the system. These mergers result in the production of a significant PV feature that leaves the West African coast and rapidly undergoes tropical cyclogenesis.

1. Introduction

African easterly waves (AEWs) are the dominant synoptic weather systems in West Africa and the tropical Atlantic during boreal summer. Characterized by 2–5-day periods and wavelengths of the order of 3000 km (Carlson 1969a), AEWs are an important component of the regional climate. They modulate West African rainfall, including mesoscale convective systems (MCSs) (e.g., Payne and McGarry 1977; Fink and Reiner 2003), they are the main precursors of tropical cyclones in the Atlantic (e.g., Avila and Pasch 1992), and may even contribute to tropical cyclogenesis in the Pacific (e.g., Frank 1970). Despite their importance, we lack a thorough understanding of the nature of AEWs, including how these systems are initiated, how they grow, and most importantly how they interact with convection, including MCSs. The analysis presented in this paper is focused on improving our understanding of these processes by considering the life cycle of an observed intense AEW from the time of its initiation in central North Africa to the time it leaves the West African coast.

It is generally accepted that AEWs arise from an instability of the midtropospheric African easterly jet (AEJ), a prominent feature of the summertime circulation over North Africa. Burpee (1972) was first to demonstrate that the AEJ satisfies the necessary conditions for baroclinic and barotropic instability (Charney and Stern 1962). Modeling studies (e.g., Thorncroft and Hoskins 1994a,b) have shown that baroclinically and barotropically growing waves are produced on an idealized midtropospheric jet and have structures that are similar to composite AEWs (e.g., Burpee 1974; Reed et al. 1977). Idealized models and composite studies emphasize the synoptic-scale features associated with AEWs. Consistent with baroclinically growing systems, AEWs have vorticity anomalies at two locations: one at low levels on the southern fringe of the Sahara (in the vicinity of the low-level potential temperature contrasts) and one at AEJ level in the rainy zone on the south side of the AEJ (in the vicinity of the potential vorticity sign reversal; cf. Pytharoulis and Thorncroft 1999).

Based on automatic tracking of vorticity centers in European Centre for Medium-Range Weather Fore-

Corresponding author address: Gareth J. Berry, ES-333, Department of Earth and Atmospheric Sciences, The University at Albany, State University of New York, 1400 Washington Ave., Albany, NY 12222.
E-mail: gareth@atmos.albany.edu

casts (ECMWF) analyses, Thorncroft and Hodges (2001) showed that two distinct storm tracks exist over the African continent, corresponding well to the location of vorticity maxima presented in the composite AEWs. It is important to note that the southern vorticity track is also a favored region for MCSs (Hodges and Thorncroft 1997), which can produce mesoscale vorticity anomalies. It is unclear how many of the tracked vorticity anomalies are associated with large MCSs and how many are associated with AEWs that develop via Rossby wave interactions. The nature of the interactions between synoptic-scale vorticity anomalies associated with AEWs and the mesoscale vorticity anomalies associated with MCSs is at the heart of the scale interaction problem.

The AEW composite based on phase III of the Global Atmospheric Research Program (GARP) Atlantic Tropical Experiment (GATE) (Reed et al. 1977) has dominated our perception of AEWs until the present day. It is important to recognize that such composites show a smoothed-out picture of a mature AEW over West Africa and provide little or no information about the physical processes and scale interactions that take place during the evolution of the system. We continue to lack a fundamental understanding of the relative roles of the synoptic-scale flow, the embedded mesoscale and subsynoptic-scale vorticity anomalies, and convection in the evolution of these systems.

We argue that more case-study work is required to consider the interactions between the synoptic scales and mesoscales. Remarkably little case-study work has been attempted since Carlson (1969a,b), as most AEW research has tended to take a modeling (e.g., Thorncroft and Hoskins 1994a) or statistical approach (e.g., Duvel 1990). In this paper we use a case-study approach to describe the evolution of an intense AEW from its initiation in central North Africa (near 11°N, 23°E) on 30 July until it crosses the West African coast on 3 August 2000 (see Fig. 1 for map of the region). This system was the strongest AEW in the summer of 2000, and within approximately 6 h of crossing the West African coast this AEW was identified as Tropical Depression 3 by the National Oceanic and Atmospheric Administration (NOAA) Tropical Prediction Center (TPC;Bevan 2000). Rapidly this depression developed into the first tropical cyclone of the 2000 season, Hurricane Alberto.

The Alberto case was considered recently by Hill and Lin (2003). Their study focused on an MCS that was triggered over the Ethiopian highlands on 28 July 2000. They argue that this event was crucial for the subsequent development of Alberto in the eastern Atlantic Ocean. Our analysis takes a much closer look at the synoptic evolution during this period, focusing more on the interactions of the synoptic-scale AEW and the MCSs and also highlighting the triggering of multiple MCSs within the evolving AEW structure.

In this study our primary source of data is the ECMWF operational analyses, which have a spatial resolution of 1.125° × 1.125° and a temporal resolution of 12 h. We also make use of satellite imagery from Meteosat. Recognizing that tropical North Africa is a data-sparse region, we will include analysis of in situ synoptic observations in order to corroborate what is seen in the numerical analyses and to examine the effect the passage of an intense AEW has on the local conditions.

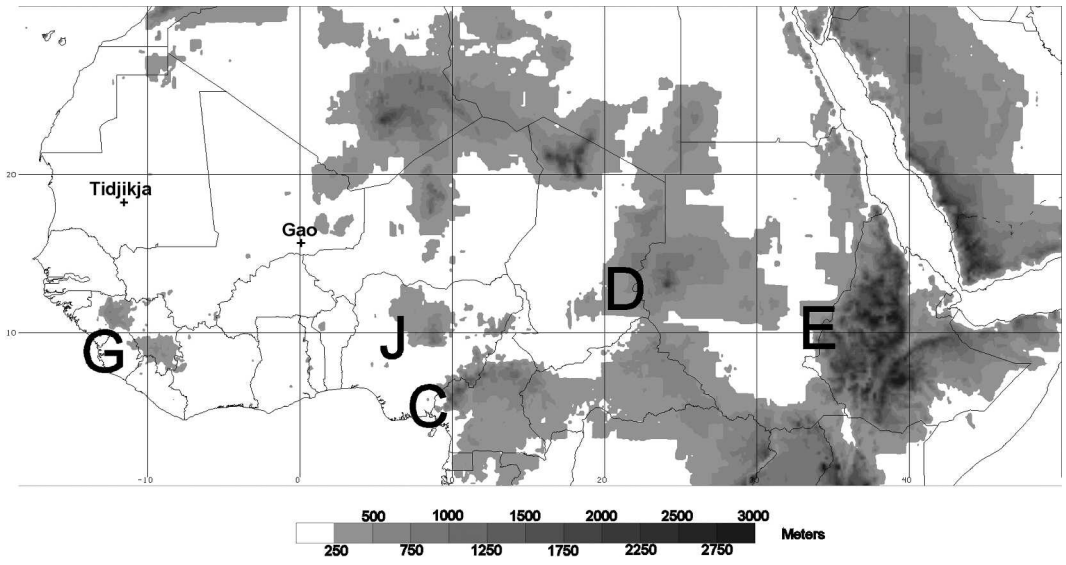

FIG. 1. Map of North Africa, including coastline and national borders. Relief over 250 m is shaded, with key at the bottom of the figure. Labels on the western side of orography identify the following regions: G = Guinea highlands, J = Jos Plateau, C = Cameroon highlands, D = Darfur highlands, and E = Ethiopian highlands. Locations of synoptic observations are marked by a cross and labeled with the station name.

This paper is organized as follows: section 2 provides an overview of the AEW being studied including the mean state of the atmosphere over tropical North Africa during summer 2000. Section 3 presents an analysis of the satellite imagery and wind field, and section 4 analyzes potential vorticity (PV) and potential temperature (θ) structure. The main results from the analysis are discussed in section 5, where a new framework for considering AEW life cycles is presented. A summary and final comments are presented in section 6.

2. Overview of the season

Figure 2 shows a Hovmöller space–time diagram of unfiltered meridional wind (v) averaged between 5°N and 15°N at 700 hPa over the African continent for July, August, and September 2000. The smooth nature of the meridional wind, compared to vorticity and potential vorticity, and the latitudinal averaging means that Fig. 2 tends to emphasize the synoptic-scale (Rossby wave type) signal of AEWs. From Fig. 2 it can be seen that waves propagate westward across the African continent, and most begin between 10° and 20°E and continue into the Atlantic Ocean. These systems move across the continent every 2–5 days, have wavelengths of order 3000 km, and phase speeds in the region of 10–15 m s^{-1}, all typical of previously observed AEWs (e.g., Reed et al. 1977).

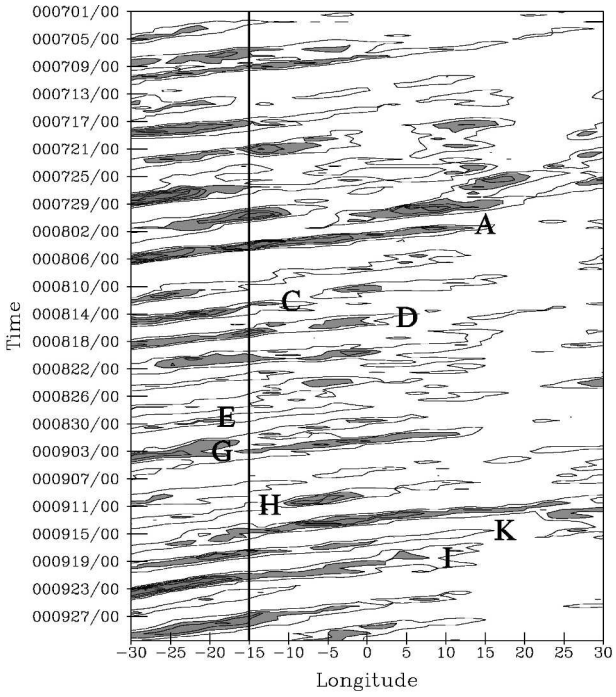

FIG. 2. Hovmöller diagram of 700-hPa unfiltered meridional wind, averaged between 5°N and 15°N for the period 1 Jul–30 Sep 2000. Only positive values are contoured, and values in excess of 2 m s^{-1} are shaded. A line is drawn at 15°W to depict the approximate position of the West African coast. The letters refer to the first letter of the named tropical cyclone that may be associated with each AEW, e.g., A = Hurricane Alberto [determined using the preliminary storm reports from the NOAA Tropical Prediction Center (http://www.nhc.noaa.gov/2000.html)].

The TPC identified many AEWs during this season as precursors to tropical cyclones; features matching information in TPC reports are labeled in Fig. 2. Note that at least 9 out of the season total of 14 tropical cyclones are attributed to AEWs, including all 3 major (category 3 or above) hurricanes. The most outstanding feature in Fig. 2 is an AEW that has a (positive) meridional wind signature that begins near 15°E on 1 August and crosses the West African coast (near 15°W) on 4 August. It is most notable due to its strength and coherency when compared to the other AEWs of the season, which is the primary reason for this event forming the basis of this case study.

Before considering the intense AEW in detail, we first consider the basic state in which it evolved. The basic-state variables are computed for the period 16 July–15 August, forming a 1-month period centered on the passage of this AEW. The mean zonal wind at 700 hPa for this period is shown in Fig. 3a. The core of the AEJ is around 12°–14°N over most of the continent and close to 17°N over the Atlantic Ocean. The jet is strongest on the West African coast with a peak speed of 11m s^{-1}, but easterly winds can be seen to stretch as far back as Ethiopia. The mean PV on the 315-K potential temperature surface for this period is shown in Fig. 3b. In this study we have chosen the 315-K potential temperature surface on which to examine the PV evolution. This level intersects the AEJ over West Africa, and perturbations and gradients are maximized near this level (cf. Thorncroft and Hoskins 1994a; Dickinson and Molinari 2000). The most prominent PV feature in Fig. 3b over the African continent is a strip of high PV that extends from Ethiopia westward into the Atlantic Ocean, centered on approximately 10°N. The existence of this strip results in a local reversal in the sign of the meridional PV gradient and is consistent with cyclonic shear on the southern flank of the AEJ. Over the desert regions, the PV is close to zero, consistent with dry convection in this region creating almost zero static stability (Thorncroft and Blackburn 1999).

Figure 3c shows the mean potential temperature (θ) at 925 hPa for this period. A strong positive θ gradient is present between 10° and 20°N over the whole of Africa. This mean positive meridional θ gradient is consistent with the observed easterly shear, and its maxima is collocated with a mean negative PV gradient (at 315 K), implying that this basic state can support the baroclinic and barotropic growth of AEWs across the whole of tropical North Africa.

Mean equivalent potential temperature (θ_e) at 925 hPa is shown is Fig. 3d. This shows that the maximum θ_e values occur in an east–west-oriented strip across central and West Africa, approximately centered on 15°N. Lowest θ_e values occur along the Gulf of Guinea coast

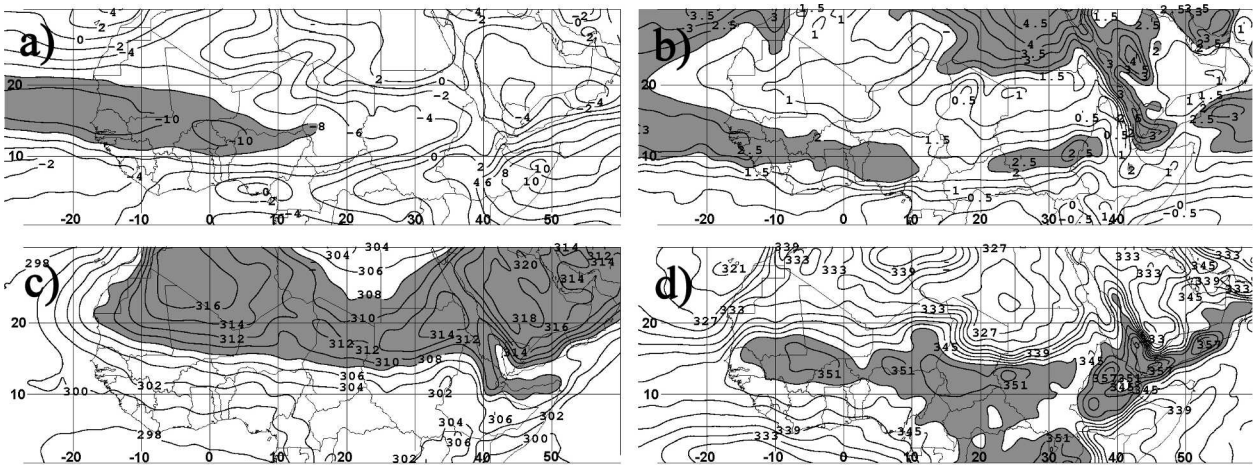

FIG. 3. The 16 Jul–15 Aug 2000 mean: (a) zonal wind at 700 hPa; contoured every 2 m s^{-1}, shaded below –8 m s^{-1} (easterlies defined as negative). (b) Ertel potential vorticity on a 315-K potential temperature surface (scaled by 10^7); contoured every 0.5×10^{-7} K kg^{-1} m^2 s^{-1}, values above 2×10^{-7} K kg^{-1} m^2 s^{-1} shaded. (c) Potential temperature at 925 hPa (averaged using 0000 and 1200 UTC analysis times); contoured every 2 K, with values in excess of 308 K shaded. (d) Equivalent potential temperature at 925 hPa (averaged using 0000 and 1200 UTC analysis times); contoured every 3 K, with values in excess of 348 K shaded.

and in the Sahara Desert, as θ_e is the product of both temperature and moisture content. Here we use θ_e as a crude proxy for convective available potential energy (CAPE) in the diagnosis of where convection is more likely to occur (cf. Williams and Renno 1993). This assumption is supported by the fact that this θ_e strip corresponds well to composite July and August MCS feature density presented by Hodges and Thorncroft (1997, see their Fig. 12).

The presence of a strip of high θ_e and low-level vertical wind shear associated with the AEJ implies that this time-mean basic state is able to support long-lived MCSs in addition to AEWs, although both can exist without the other. This will now be considered in the context of our case study.

3. Synoptic analysis of the AEW life cycle

a. Satellite observations

In addition to the strong signature in the meridional wind field (Fig. 2), this system was associated with a coherent westward moving convective signature, which is shown by a mosaic of water vapor (WV) imagery in Fig. 4. A very distinct signal can be tracked in the WV imagery from an initial region of convection on 30 July, evolving through several stages and moving off the African coast on 3 August 2000.

The initial convection occurs around 0300 UTC on 30 July 2000 (Fig. 4, between frames 1 and 2) near 11°N, 23°E. This is a mountainous area in the southern part of the Darfur region of western Sudan (see Fig. 1), located just to the south of the maximum 925-hPa mean temperature gradient (Fig. 3c) and a region favored for the initiation of long-lived mesoscale convective weather systems (Hodges and Thorncroft 1997). Interestingly, this convection is initiated at a time of day (approximately 0600 local time) when mean MCS genesis frequency over Africa has been shown to be a minimum (Hodges and Thorncroft 1997). Note that the initial convection (henceforth referred to as the first convective burst) is located east of and earlier than the first location of the AEW shown in the Hovmöller diagram of meridional wind (Fig. 2). This suggests that this convection acts as the precursor for the AEW that develops downstream.

Subsequent satellite images show that this convective region rapidly develops, with high clouds covering a region in excess of 1000 km across by 1800 UTC on 30 July 2000 (Fig. 4, frame 4). The brightness of the pixels in Fig. 4 indicates that the amount of very deep convection begins to decay 18 h after the initiation, by which time the center of the convective region is close to 10°E (Fig. 4, frame 5). There is a reduced amount of deep convection within the convective region for the following 12 h as it moves over western Chad, northern Cameroon, and into eastern Nigeria (Fig. 4, frames 5–7). Deep convection occurs on the leading edge of the remnants of the first convective burst along the Gulf of Guinea coast (Fig. 4, frame 8), but decays after approximately 12 h, consistent with movement into a region of lower mean θ_e near the coast (cf. Fig. 3d) (see Thorncroft and Haile 1995). At the same time as this decays (0600 UTC 1 August 2000; Fig. 4, frame 10) another localized region of deep convection develops over central Nigeria, near the Jos Plateau (see Fig. 1), marking the start of the second convective growth cycle over Africa (this event will henceforth be referred to as the second convective burst).

After the second convective burst the region of con-

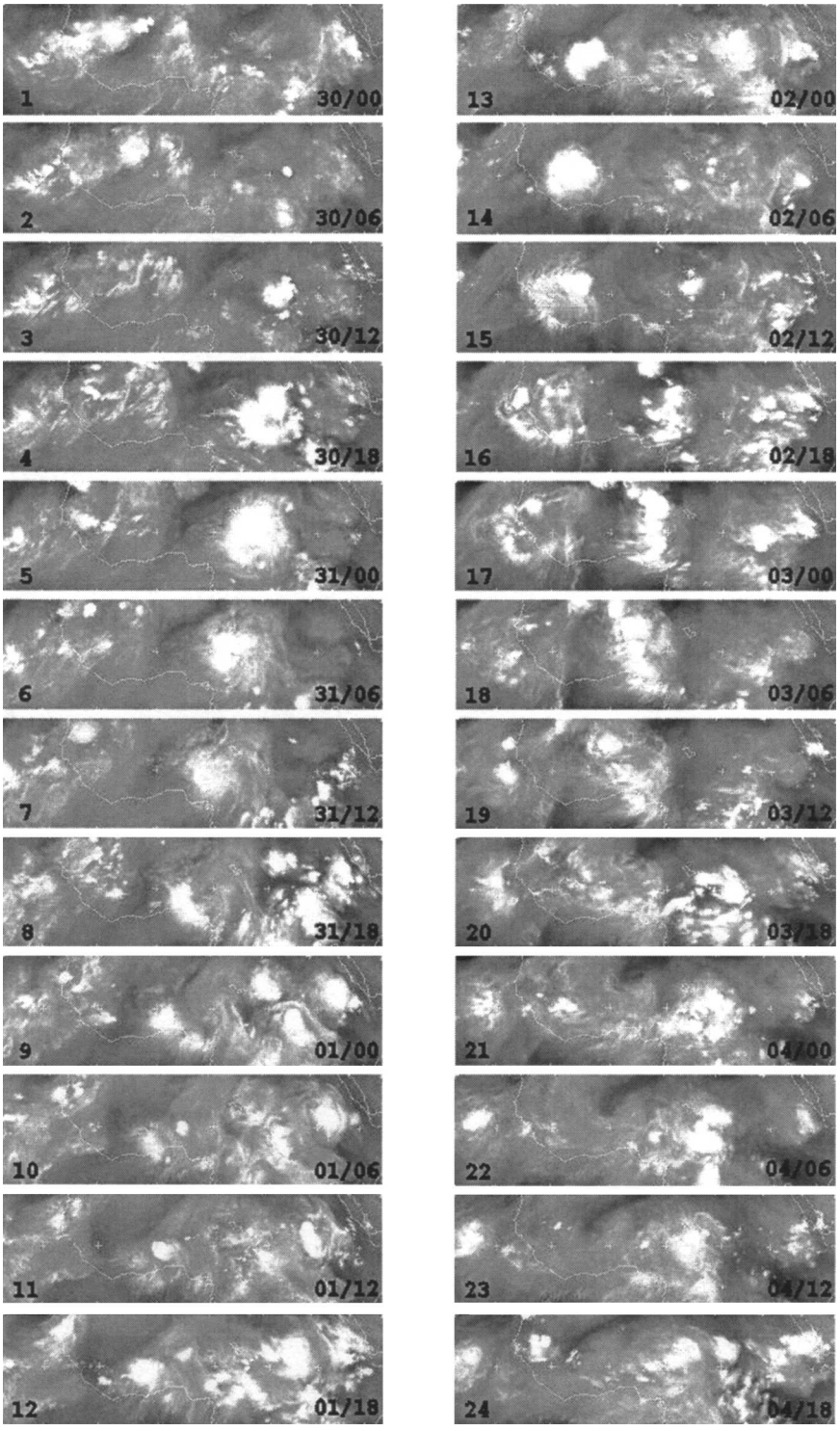

FIG. 4. Mosaic of water vapor imagery from *Meteosat-7* for the period 30 Jul–4 Aug 2000. Latitude–longitude crosses are shown every 10°, and the African coast is outlined. The date of each image is shown in the bottom right of each frame (in day–hour format), and each frame is numbered in bottom left for reference. Images copyright 2004 by EUMETSAT.

vection continues to move westward and expands. Note the second convective burst occurs close to the beginning of the meridional wind signal in the Hovmöller diagram (Fig. 2), suggesting possible interactions between the AEW and convection. Water vapor and infrared (not shown) imagery suggest that the region of convection reaches its peak over the Ivory Coast (near 10°N, 5°W) on 2 August 2000 at approximately 0000 UTC. (Fig. 4, frame 13). From this point, the large region of deep convection appears to decay into a number of smaller mesoscale regions of convection, embedded within an "envelope" of higher humidity that continues to move westward (Fig. 4, frames 14–17). These mesoscale regions of convection cross the West African coast between 0000 UTC and 1200 UTC on 3 August (Fig. 4, frame 17 onward), and some appear to develop over the ocean. At 1800 UTC on 3 August, the TPC best-track data places Tropical Depression 3 at 10.8°N, 18.0°W (Bevan 2000), within one of these regions of convection. Twenty-four hours after crossing the African coast (approximately 0600 UTC 4 August 2000; Fig. 4, frame 22) a single coherent, cyclonically rotating cloud mass near 22°W (identified by the TPC as Tropical Storm Alberto) dominates the cloud features in this region.

In addition to this continuously evolving region of convection propagating westward, the WV imagery shows another interesting feature. Persistent localized convection occurs over the Guinea highlands (labeled "G" in Fig. 1), beginning at 1800 UTC on 1 August (Fig. 4, frame 12) and continuing until it is incorporated into the westward propagating region of convection (Fig. 4, frames 14, 15). Our analysis below suggests that interactions between the convection occurring over the Guinea highlands and the propagating convection may have played a role in the production of the offshore tropical cyclone.

In the next subsection we present a synoptic analysis of the wind and vorticity fields during the life cycle of this AEW, which will highlight the relationship between the synoptic-scale AEW and the observed convection.

b. Wind and vorticity fields

In this section we examine the evolution of the unfiltered 700-hPa meridional wind and 850-hPa relative vorticity fields during the passage of this AEW. The choice of these levels is motivated by the results from earlier studies (e.g., Reed et al. 1977; Thorncroft and Hodges 2001); the meridional wind at 700 hPa serves to highlight the Rossby wavelike aspects at the level of the AEJ, and relative vorticity at 850 hPa serves to highlight the vorticity centers that are associated with AEWs.

Figure 5 shows horizontal maps of both the 700-hPa meridional wind and the 850-hPa relative vorticity from 30 July to 3 August 2000. It is possible to see some well-defined features of the AEW from approximately 20°E westward. In the 700-hPa meridional wind field, a synoptic-scale trough is first seen over West Africa on 1 August at 0000 UTC (Fig. 5d) and moves into the Atlantic on 3 August (Fig. 5h), consistent with the information presented in the Hovmöller diagram (Fig. 2). Note that in this study, the term "trough" is used loosely to refer to a traveling, coherent north–south–oriented $v = 0$ m s^{-1} contour; this is a reasonable assumption as the mean meridional wind in the region of interest is close to zero (not shown). Comparison of the 700-hPa meridional wind and satellite imagery (Fig. 4) indicates that over the continent, the center of the observed convection is always ahead of the westward moving trough, consistent with previous composite studies (e.g., Reed et al. 1977).

At 850 hPa over the continent, a significant vorticity center at 850 hPa propagates along the baroclinic zone (see Fig. 3c) between 15° and 20°N, ahead of the 700-hPa trough. This vorticity center [henceforth referred to as the northern vortex (NV)] can first be seen on 30 July at 1200 UTC (Fig. 5a) over central Chad (approximately 17°N, 19°E). The NV can be tracked over subsequent analysis times to a position close to the West African coast (19°N, 12°W) on 3 August at 1200 UTC (Fig. 5i). Note that at the approximate time of the second convective burst (Fig. 5e) the NV becomes connected with vorticity that is associated with the observed convection. However, the continuity from the surrounding analysis times (and further analysis of the wind field at other levels) allows the NV to be tracked. It is clear that in the analysis times following the second convective burst (Figs. 5f–i) the NV significantly intensifies, moves north-northwest [approximately following the mean 925-hPa θ gradient (Fig. 3c)] and eventually dissipates near the West African coast (not shown).

Another significant 850-hPa vorticity center becomes evident over the Guinea highlands [see Fig. 1; henceforth referred to as the Guinea highlands vortex (GHV)] on 2 August at 0000 UTC (Fig. 5f). The GHV remains stationary and intensifies for the 24 h as the upstream 700-hPa trough continues to move westward. With the passage of the 700-hPa trough and observed convection (Fig. 4) the GHV moves into the eastern Atlantic Ocean, suggesting the possibility of an interaction or merger between the GHV and vorticity associated with the 700-hPa trough. It is this vorticity center that can be directly linked to Hurricane Alberto (not shown).

The analysis above has used conventional synoptic fields to identify some distinctive features of this AEW that are broadly consistent with those seen in previous studies (e.g., Reed et al. 1977). The next section adopts a potential vorticity–potential temperature (PV–θ) thinking perspective that we believe enables us to obtain a better conceptual understanding of the evolution of this system.

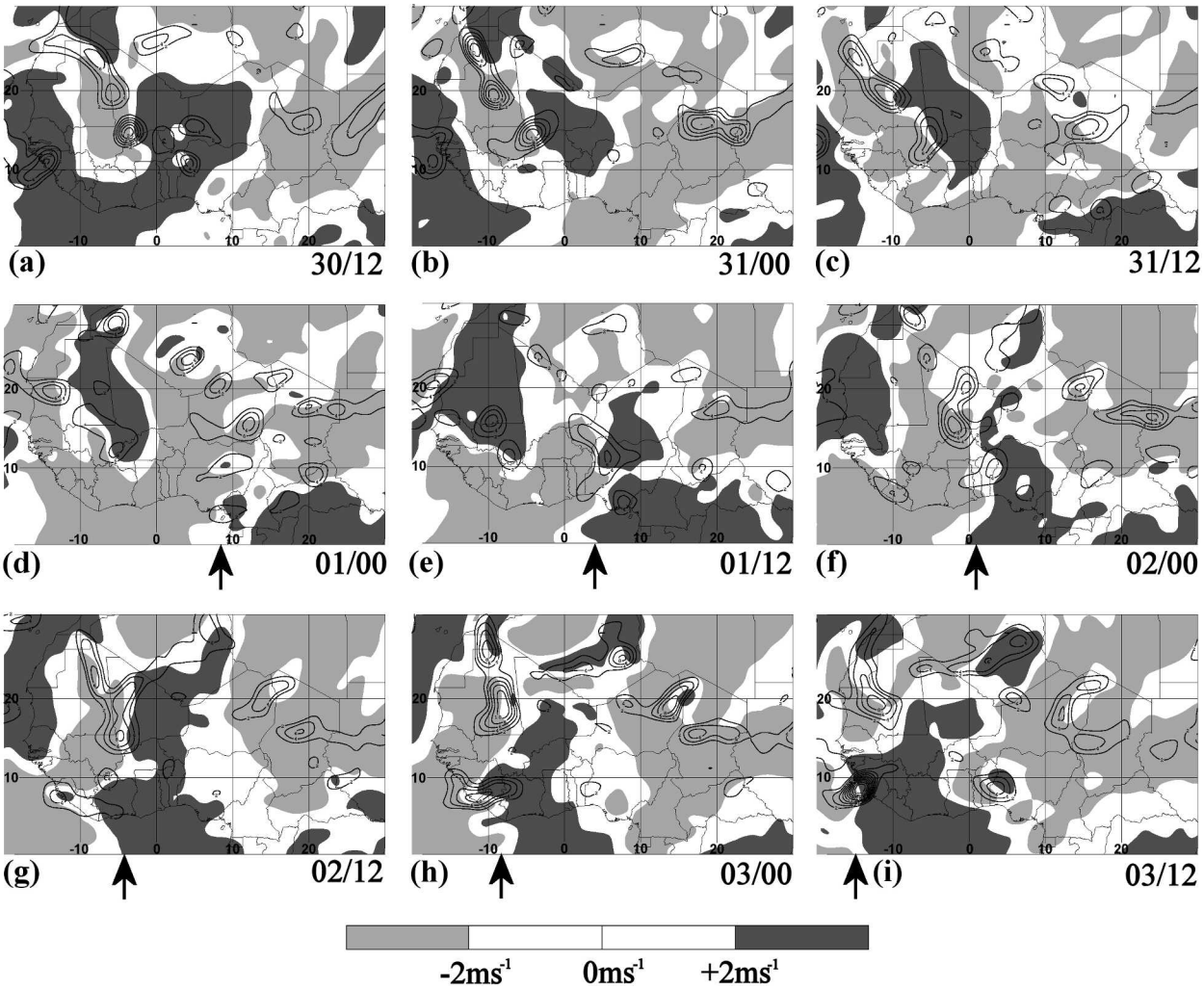

FIG. 5. Sequence of horizontal maps of 700-hPa meridional wind (shaded) and 850-hPa relative vorticity (contours) shown every 12 h from 1200 UTC on the 30 Jul 2000 until 1200 UTC on 3 Aug 2000. Areas of meridional wind in excess of 2 m s^{-1} are darker shading and those below –2 m s^{-1} are lighter shading. Relative vorticity is contoured at 2 $\times 10^{-5}$ s^{-1} intervals, beginning at $+2 \times 10^{-5}$ s^{-1}. The bold arrow at the bottom of some maps marks the subjectively estimated longitudinal position of the 700-hPa trough, and the day–hour is shown in the bottom right of each map.

4. Potential vorticity–potential temperature view

Analysis of Ertel PV on a θ surface offers significant advantages over analysis of the wind and vorticity fields in the previous section. Information about processes can be obtained since purely adiabatic processes (e.g., propagation of Rossby waves) will simply redistribute PV; diabatic processes will create or destroy PV (Hoskins et al. 1985). Consideration of the PV and θ fields together should help us to identify mechanisms that are important for the growth of this system and highlight the key scale interactions.

a. Potential vorticity–potential temperature evolution

The evolution of PV on the 315-K surface and θ at 925 hPa is shown in Fig. 6. Note that in general a meandering strip of high PV extends across west and central Africa between 5°N and 20°N. Like the time-mean basic-state PV (Fig. 3b) there is a zonally oriented strip of high PV extending across the African continent, but its day-to-day position and intensity are highly variable. During the period shown in Fig. 6, two significant positive perturbations occur on this PV strip; the first is centered over Burkina Faso (near 0°W) on 30 July at 1200 UTC (Fig. 6a) and moves northwestward, leaving the West African coast near 20°N on 1 August. The second becomes evident over Nigeria on 1 August (Figs. 6d,e) and propagates westward, increasing its amplitude with time and crossing the West African coast near 10°N on 3 August (Figs. 6h,i). Arrows at the bottom of each panel in Fig. 6 show that the axis of the second wavelike PV perturbation corresponds to the longitudinal position of the 700-hPa trough associated with the AEW being studied.

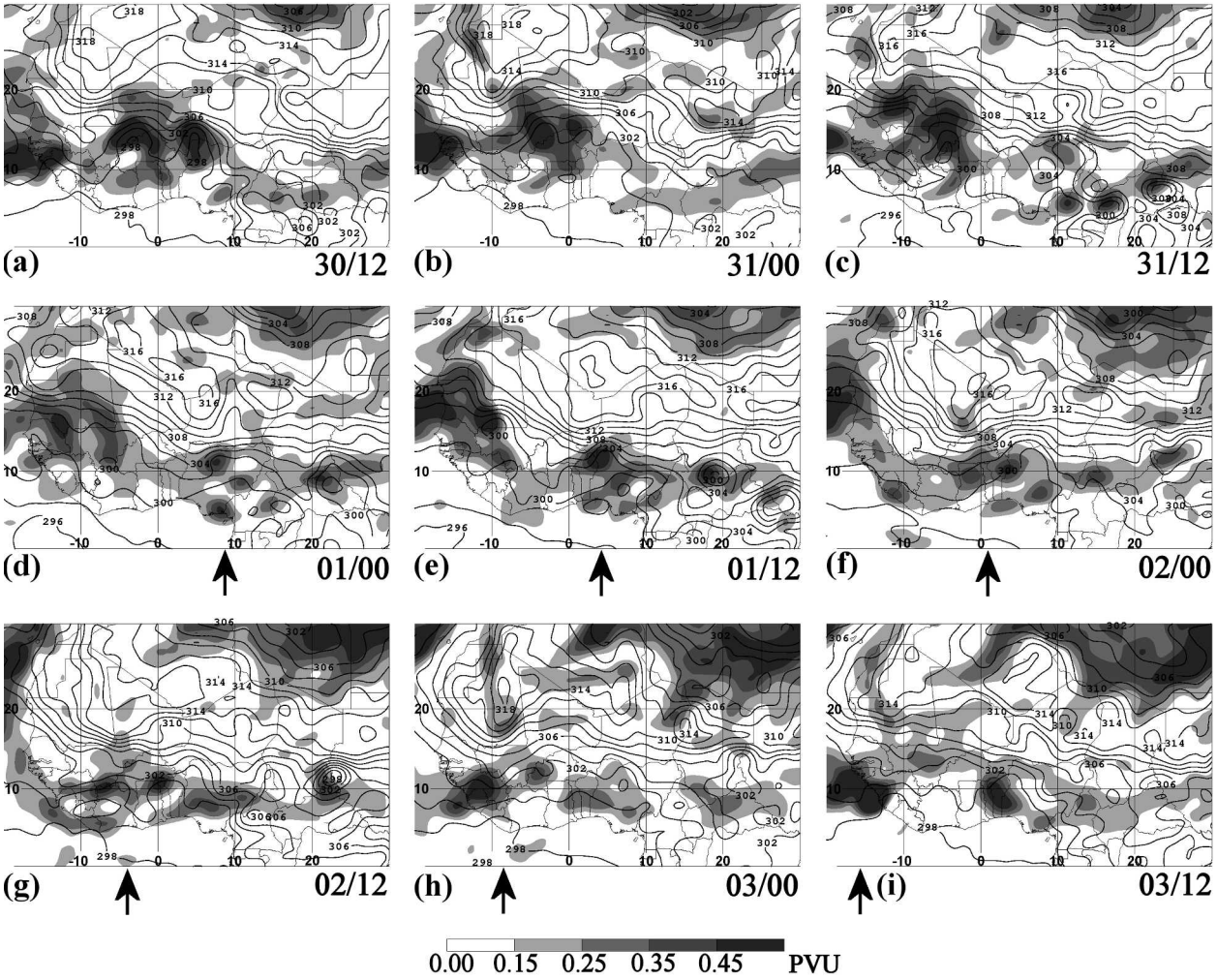

FIG. 6. Sequence of horizontal maps of 315-K potential vorticity (shaded and scaled by 10^6) and 925-hPa potential temperature (contours) shown every 12 h from 1200 UTC on 30 Jul 2000 until 1200 UTC on 3 Aug 2000 at 1200 UTC. Areas of potential vorticity in excess of $+0.15 \times 10^{-6}$ K kg^{-1} m^2 s^{-1} [0.15 potential vorticity units (PVU)] are shaded (key at the bottom of figure) and potential temperature is contoured every 2 K. The bold arrow at the bottom of some maps marks the subjectively estimated longitudinal position of the 700-hPa trough, and the day–hour is shown in the bottom right of each map.

There is clearly considerable subsynoptic-scale PV structure within both perturbations, in the form of subsynoptic-scale PV maxima that evolve as they move westward. These are most likely to be the result of latent heat release from deep convection as the approximate timing and location of the appearance of these maxima are generally consistent with the analysis of the observed convection (Fig. 4) and analyzed vertical motion at 400 hPa (not shown).

The 925-hPa θ structure in Fig. 6 is more similar to its time mean (Fig. 3c) than the PV field as it has less pronounced short-term variation, but it is clear that during the period shown significant westward propagating wavelike disturbances are seen on the strong meridional θ gradient that exists on the southern fringe of the Sahara. It is also clear that these two disturbances move coherently with the two perturbations on the 315-K PV strip, and Fig. 5 shows that these disturbances are collocated with 850-hPa vorticity centers over West Africa.

From Fig. 6, it is evident that during the period 0000 UTC on 1 August to 1200 UTC on 2 August (Figs. 6d–g), the warm part of the disturbance on the 925-hPa θ gradient is located to the north and west of the positive PV perturbation on the PV strip. Noting that the flow anomaly associated with the perturbation on the PV strip is the sum of the contribution of the perturbation and its embedded PV maxima; this is a configuration that is consistent with baroclinic growth (e.g., Hoskins et al. 1985).

Subsynoptic-scale PV maxima are generated over the Guinea highlands from 2 August at 0000 UTC (Fig. 6f), consistent with the observed convection and the appearance of the GHV in the relative vorticity field. As

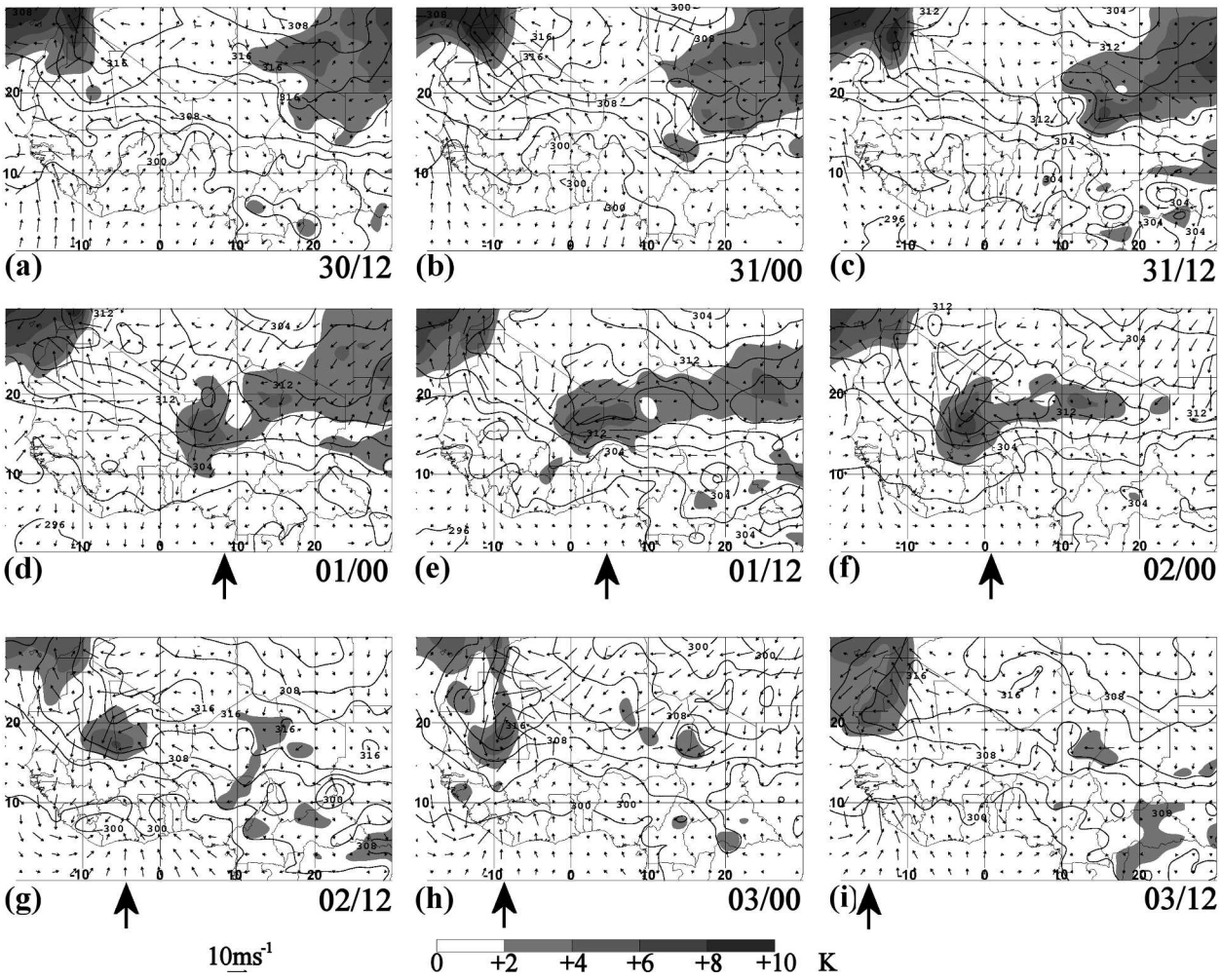

FIG. 7. Sequence of horizontal maps every 12 h from 1200 UTC on 30 Jul 2000 until 1200 UTC on 3 Aug 2000 at 1200 UTC showing 925-hPa potential temperature anomaly (K, shaded) and wind anomaly (vectors) from 16 Jul–15 Aug means. Potential temperature at 925 hPa is also shown, contoured every 4 K. All 0000 UTC anomalies are show relative to a mean calculated using only 0000 UTC analysis times, and all 1200 UTC anomalies are show relative to a mean calculated using only 1200 UTC analysis times in order to eliminate the diurnal cycle. The bold arrow at the bottom of some maps marks the subjectively estimated longitudinal position of the 700-hPa trough, and the day–hour is shown in the bottom right of each map.

the positive PV perturbation on the 315-K PV strip reaches the Guinea highlands (Figs. 6h,i), these PV maxima seem to interact with the PV maxima embedded in the positive perturbation on the PV strip. It is apparent that these PV maxima merge with one another and develop, such that at 1200 UTC on 3 August (Fig. 6i) a strong, double-centered PV maxima leaves the West African coast, rapidly becomes more symmetrical, and later becomes the PV signature of Hurricane Alberto (not shown).

b. Impact of low-level θ anomaly and northern vortex

Previous studies have often been concerned with the impact of AEWs on convection (e.g., Reed et al. 1977; Fink and Reiner 2003). This is extremely complex to investigate using observations and model analyses because of the difficulty in separating the adiabatic and diabatic signals. The analysis presented in the previous subsection has highlighted the presence of a significant disturbance to the low-level θ field in the dry region poleward of the mean AEJ that is not impacted by moist convection. Here we take a closer look at the role of the NV and consider the potential role that such a feature and its associated winds may have on convection.

Figure 7 shows horizontal maps of 925-hPa θ anomalies (with diurnal cycle removed) and 925-hPa wind anomalies from the 16 July–15 August mean. At the beginning of this period large-scale warm anomalies exist in extreme northeast and northwest Africa. Further analysis (not shown) indicates that these large-scale anomalies are connected with midlatitude troughs that

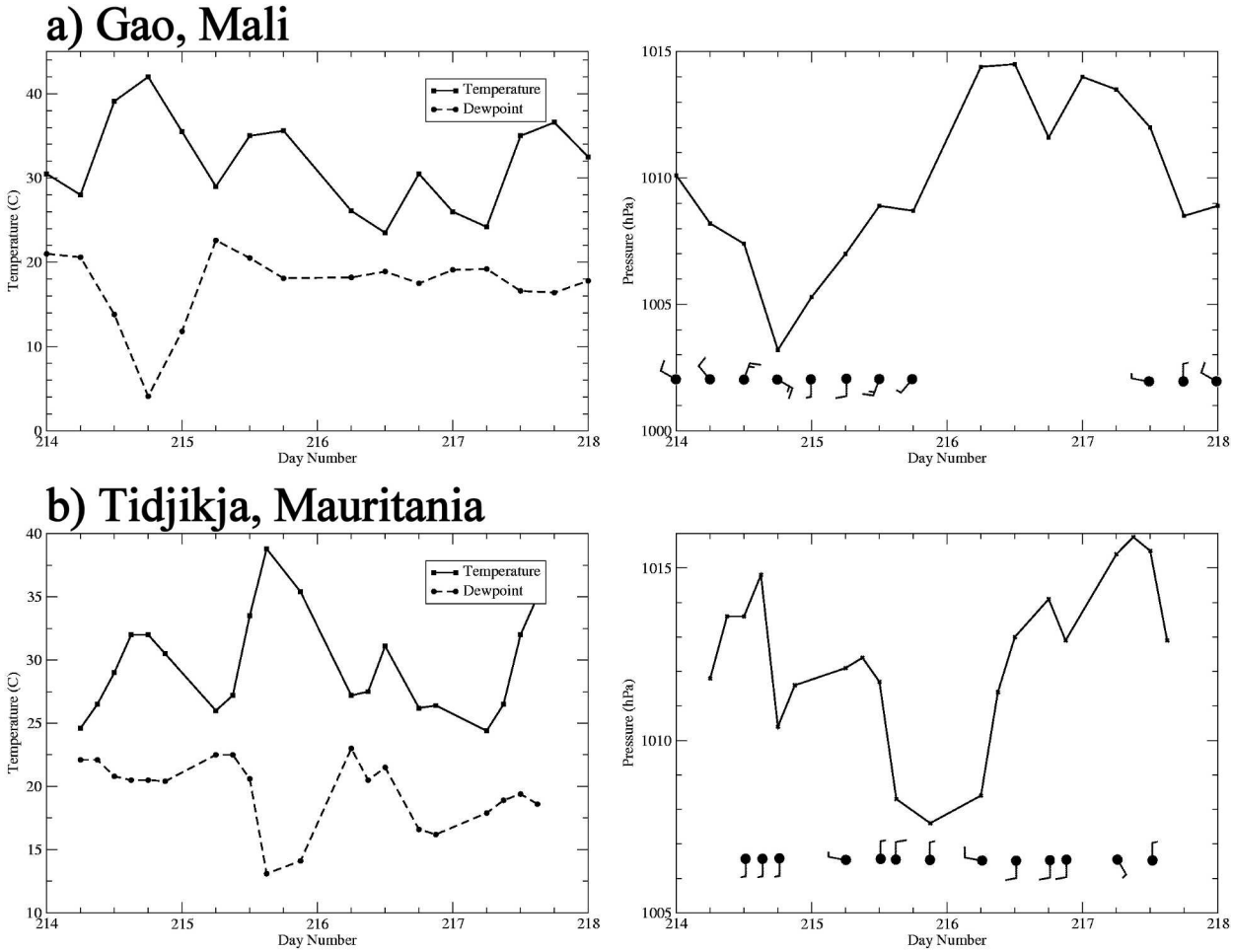

FIG. 8. (left) Time series of temperature and dewpoint along with (right) sea level pressure and surface wind (winds shown to the nearest 5 kt; half barb is 5 kt, full barb is 10 kt) for synoptic stations at (top) Gao, Mali (16.3°N, 0.1°W), and (bottom) Tidjikja, Mauritania (18.6°N, 11.4°W), for the period 0000 UTC on 1 Aug 2000 (day number 214) until 0000 UTC on 5 Aug 2000 (day number 218).

protrude into the northern part of this region. Prior to the first convective burst on 30 July (not shown) winds associated with a midlatitude trough advected warm air from the central Sahara to create a large area of positive θ anomalies in the eastern half of the Sahara. After the first convective burst it is evident from Figs. 7a–i that a synoptic-scale warm anomaly with a cyclonic circulation (the NV) emerges from the large-scale warm anomaly and moves across the African continent with the passage of this AEW. Consistent with the 850-hPa relative vorticity field (Figs. 5a–i), a weak anomalous cyclonic circulation becomes distinct on 31 July at 0000 UTC (Fig. 7b) over northern Chad, strengthens near the Greenwich meridian (Fig. 7e) and reaches the West African coast (Fig. 7i), where it subsequently dissipates (not shown). What is significant about this feature is the large extent and strength of the anomalous cyclonic winds that are centered on it over West Africa. Near the Greenwich meridian (Fig. 7f) the θ anomaly exceeds 7 K from 16 July–15 August 0000 UTC mean and low-level wind anomalies of nearly 20 m s^{-1} exist near the center of this feature. The anomalous circulation extends over the location of the perturbation to the PV strip (see, e.g., Fig. 6f), indicating that the observed meridional extension of the positive perturbation to the 315-K PV strip and maintenance of θ anomaly is consistent with baroclinic interaction.

Given the large low-level amplitude of the NV and associated warm anomaly in the ECMWF operational analysis, we would expect to see evidence of this feature in synoptic observations. Figure 8 shows time series of surface observations from Gao, Mali (16.3°N, 0.1°W) (Fig. 8a) and Tidjikja, Mauritania (18.6°N, 11.4°W) (Fig. 8b) for the period 0000 UTC on 1 August (day number 214) to 0000 UTC on 5 August (day number 218). These stations, whose positions are shown in Fig. 1, lie approximately along the intense mean meridional θ gradient (Fig. 3c) and are close to the path of the NV.

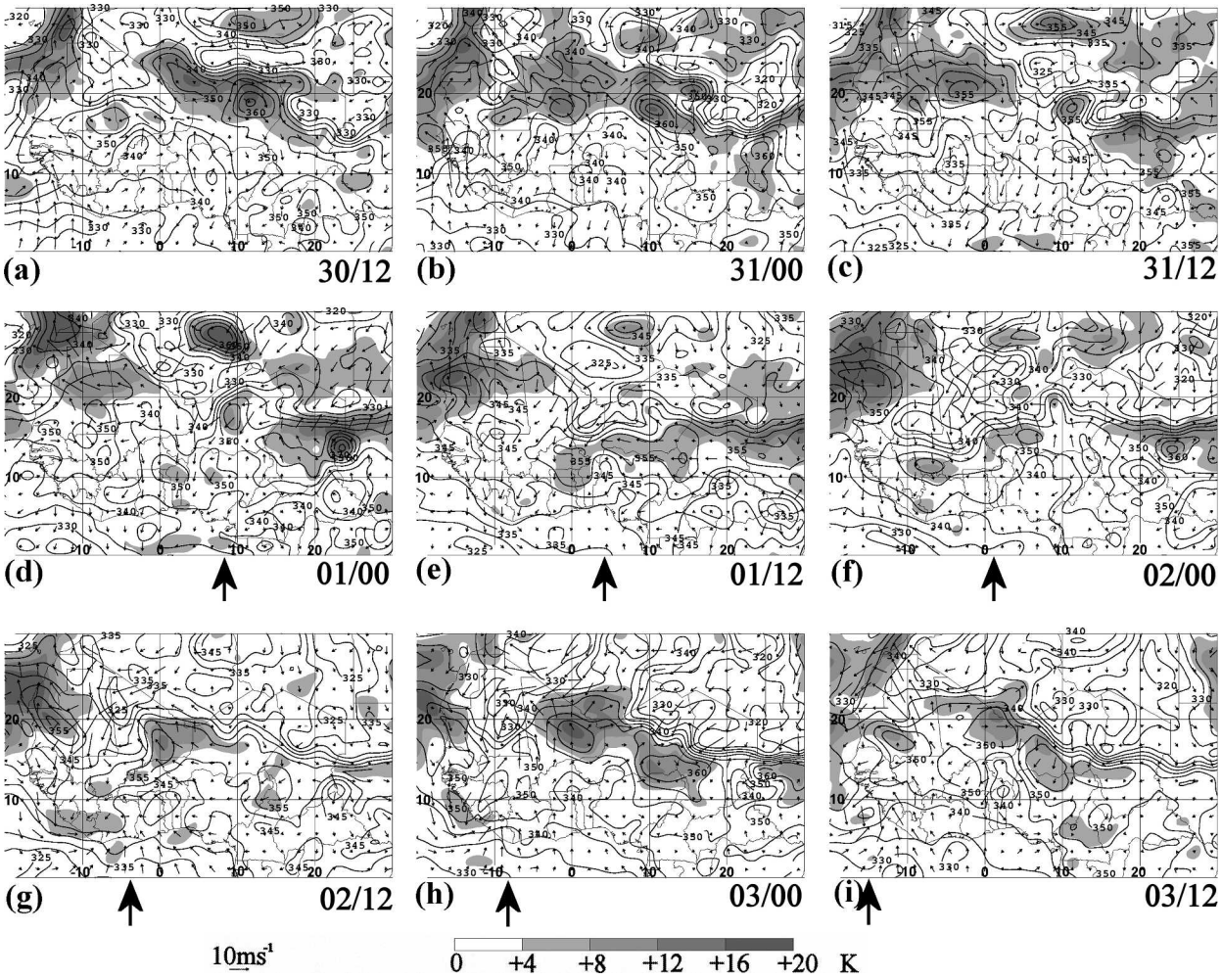

FIG. 9. Sequence of horizontal maps every 12 h from 30 Jul 2000 at 1200 UTC until 3 Aug 2000 at 1200 UTC showing 925-hPa equivalent potential temperature anomaly (K, shaded) and wind anomaly (vectors) from 16 Jul–15 Aug means. Equivalent potential temperature at 925 hPa is also shown, contoured every 5 K. All 0000 UTC anomalies are show relative to a mean calculated using only 0000 UTC analysis times, and all 1200 UTC anomalies are show relative to a mean calculated using only 1200 UTC analysis times in order to eliminate the diurnal cycle. The bold arrow at the bottom of some maps marks the subjectively estimated longitudinal position of the 700-hPa trough, and the day–hour is shown in the bottom right of each map.

The ECMWF operational analyses indicate the NV passes Gao on 1 August (day number 214) and at Tidjikja on 2 August (day number 215). The passage of this feature is clearly marked at both stations by a significant increase in temperature coupled with a drop in dewpoint, a pressure minimum, and a wind shift from northerly to southerly. Supplementary observations such as a drop in visibility and the absence of significant low clouds lead us to conclude that the source of this air is the desert region to the north. Given the potential impact of the NV on convection to the south, it is plausible that these strong signals could be useful real-time indicators of a baroclinically growing AEW and have a potential use as a forecasting tool.

To consider the possible consequences of this strong low-level circulation on the observed convection, a sequence of θ_e and θ_e anomaly maps at 925 hPa are shown in Fig. 9. Recall from the mean shown in Fig. 3d that the NV moves along the northern edge of the high θ_e strip that extends across the African continent. Figure 9 suggests that the strengthening circulation of the NV distorts the θ_e structure over West Africa by advecting the θ_e strip, creating a quadrapole of θ_e anomalies (Figs. 9d–g), seen particularly clearly centered near 15°N, 3°W in Fig. 9f. It is evident in Fig. 9 that equatorward of the mean θ_e strip, positive anomalies occur in the northerly flow associated with the NV (i.e., ahead of the 700-hPa trough), whereas poleward of the mean high θ_e strip positive anomalies occur in the southerly flow associated with the NV (see, e.g., Figs. 9f,g). Note that prior to the passage of the NV (Figs. 9a–c), there are no significant positive θ_e anomalies in this region. This ad-

vection of θ_e is important since modifying the low-level environment increases the probability of convection where positive low-level anomalies occur. Using Fig. 4 of Williams and Renno (1993) as a guide, we roughly estimate that CAPE increases of the order of 1000–2000 J kg^{-1} occur over a 24-h period ahead of the region of convection [consistent with changes in CAPE in soundings from Bamako, Mali (not shown)]. Indeed, similar reasoning can be applied to the convection observed over the Guinea highlands, where it is plausible that the continual southward advection of high θ_e air by the flow associated with NV over the topography increases the probability of convection there. This analysis is suggestive of the fact that low-level advection of θ_e by the NV can impact the stability of the environment and therefore convection. More detailed analysis is required to investigate this, including a more thorough exploration of boundary layer budgets of θ_e and an examination of how mesoscale convection can affect the θ_e structure in the vicinity of AEWs.

The location of the positive θ_e anomalies relative to the 700-hPa trough are consistent with the observations of regions of enhanced convection from previous composite studies (e.g., Reed et al. 1977; Fink and Reiner 2003). These studies showed that enhanced convection primarily occurs west of the trough in the southern region of AEWs with a secondary peak east of the trough in the northerly regions.

5. Discussion

Based on our analysis in the previous sections and previous studies cited in the introduction, a conceptual framework for describing the evolution of AEWs from initiation until reaching the east Atlantic is now presented. Our analysis promotes the division of the life cycle of AEWs into three distinct phases:

(i) initiation,
(ii) baroclinic development, and
(iii) west coast developments.

A schematic that highlights the key aspects of these phases is shown in Fig. 10. As far as the results from our study and previous work allow, each phase will be discussed below.

a. Phase (i): Initiation

Because of sparse observations east of approximately 10°E and a very small number of papers on initiation (e.g., Albignat and Reed 1980) we know very little about this phase of the AEW life cycle. Here, we have indicated that the genesis of this AEW is associated with a large region of convection that began in the Darfur region of Sudan. Previous studies (e.g., Burpee 1972; Hodges and Thorncroft 1997) suggest that the orography in eastern and central Africa is important for the genesis region for both AEWs and long-lived

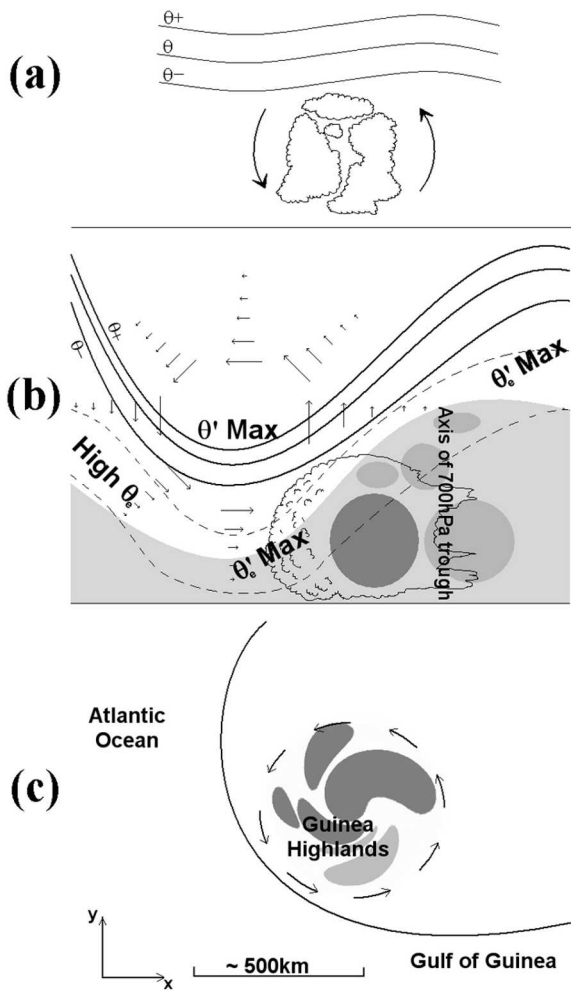

FIG. 10. Schematic showing the evolution of an AEW. (a) Initiation [phase (i)]: the low-level potential temperature (θ) contours are depicted as solid lines oriented along the x axis, with higher values (denoted $\theta+$) existing in the direction of the positive y axis. The region of convection is depicted as a cartoon cloud, and arrows show the hypothesized low-level flow anomaly associated with it. (b) Baroclinic development [phase (ii)]: thick black lines indicate low-level potential temperature contours with higher values (denoted $\theta+$) existing in the direction of the positive y axis. The axis of the high equivalent potential temperature (θ_e) strip falls between the two dashed contours and is labeled. The arrows show the anomalous wind at low levels, with the length of the each arrow being indicative of the wind speed. The θ'Max and θ_e'Max labels indicate regions of maximum low-level θ and θ_e anomalies. The AEJ-level potential vorticity distribution is shown by the shading—the lightest tone indicates the adiabatically redistributed PV of the mean PV strip, the middle tone indicates PV maxima that were generated by earlier convection, and the darkest tone indicates PV that is associated with active convection (which is depicted as a cartoon cloud). The position of the 700-hPa trough line (defined using the meridional wind field) is added for reference. (c) West coast development [phase (iii)]: the black outline depicts the West African coast, and major geographical features are labeled. The AEJ-level PV maxima associated with westward propagating convection are indicated by darker shading, and those associated with convection over the Guinea highlands are indicated by lighter shading. The arrows indicate the sense of the AEJ-level circulation. An approximate scale is included at the bottom of this figure.

MCSs. Indeed, the recent study by Hill and Lin (2003) suggests that the system that eventually evolves into Hurricane Alberto has its origins as an MCS over the Ethiopian Highlands two days before the first convective burst in our study. Using Meteosat IR imagery (not shown), we have noted a decaying small-scale (order 200 km) circulation in the remnant low clouds of this MCS east of Darfur, some 12 h before the first convective burst. It is plausible that the MCS identified by these authors played a role in triggering the first convective burst (e.g., by remnant midtropospheric PV or an outflow boundary providing an initial lifting mechanism), but our analysis strongly suggests that the genesis of this AEW is associated with the first convective burst over Darfur.

We hypothesize that the AEW life cycle begins by the unstable basic state being perturbed by a large region of convection that is triggered over the elevated terrain of Darfur. As seen in the satellite image on 30 July 2000 (Fig. 4, frames 2–5) and illustrated in the schematic in Fig. 10a, this convection grew rapidly to cover a very large region that represents a large area of heating (Houze 1989), which we would expect to lead to a significant perturbation to the wind field (e.g., Mapes 1998). The dynamical response to this heating on the unstable basic state could subsequently result in downstream development of baroclinically and barotropically growing AEWs (cf. Simmons and Hoskins 1979).

This phase of the life cycle highlights deficiencies in model analyses of this data-sparse region, which leads to uncertainties in our analysis and prevents a more definitive investigation. For example, the model analysis does not produce a PV or wind signature in the region of convection until the second convective burst, despite evidence for circulation in animations of satellite imagery. However, we are confident that a coherent perturbation to the θ gradient (and associated NV) is produced close to the first convective burst. This perturbation becomes an important component of the next phase of the life cycle.

b. Phase (ii): Baroclinic development

The second phase of the AEW life cycle (illustrated schematically in Fig. 10b) commences as the synoptic-scale perturbation to the θ gradient begins to interact with a synoptic-scale perturbation to the AEJ-level PV strip. For approximately 2 days over West Africa, these perturbations move together in a configuration that is consistent with baroclinic growth, and both perturbations are observed to amplify.

Our analysis clearly shows that isolated PV maxima are generated within the positive perturbation to the PV strip. These PV maxima are important since being embedded within the positive perturbation they contribute to the total AEJ-level PV anomaly. This implies that the isolated PV maxima also influence the flow anomaly associated with this perturbation [using the principle of invertibility (Hoskins et al. 1985)]. Therefore, it is likely that the contribution of the embedded PV maxima to the synoptic-scale flow could be a key factor in determining the baroclinic growth rate of this AEW. It is evident from our analysis that in general these PV maxima are diabatically generated by deep convection. Hence, it is important to examine the nature of these PV maxima in order to consider how the convection can impact the AEW.

Examination of the PV field (Fig. 6) shows that the PV maxima tend to remain coherent for a number of days, whereas the convection undergoes a series of growth and decay cycles that have a shorter time scale. It is likely that not all the PV maxima embedded in the positive perturbation to the PV strip are associated with "active" convection; many of the analyzed PV maxima could be considered "remnants" of previous convection that still add to the AEJ-level circulation anomaly. The results of Hertenstein and Schubert (1991) (which showed that in a squall-line system, midtropospheric PV production is maximized in the region of stratiform rainfall) suggest that we would expect AEJ-level PV maxima to be generated in the region of stratiform rainfall east of the deepest convection. Comparison of the satellite imagery (Fig. 4) and the maps of PV (Fig. 6) indicates that in general this is the case, although further analysis is required to determine the reason for this relationship. Note that these PV maxima tend to be generated slightly west of the position of the existing 700-hPa trough, implying that these maxima in part promote the westward propagation of the trough, as the production of PV maxima modifies the AEJ flow anomaly and redefines the position of the 700-hPa trough. This resembles the "diabatic Rossby wave" model proposed by Parker and Thorpe (1995) for the case of frontal waves and should be investigated further for the case of AEWs.

As noted in our analysis (and in previous studies), deep convection tends to be most concentrated in the region west of the 700-hPa trough. This coherent relationship between the AEW phase and convection implies that there may be some interaction or feedback between them. Our results have shown in this case that the NV moved along the northern edge of a low-level strip of high θ_e that extends across tropical North Africa, distorting it to produce positive θ_e anomalies close to the existing convection and the positive perturbation to the PV strip. This process acts to increase low-level instability in a region where low-level lifting mechanisms [e.g., outflow from existing convection, ascent resulting from the adiabatic AEW structure (Thorncroft and Hoskins 1994a)] or the embedded convectively generated PV maxima (cf. Raymond and Jiang 1990) exist. This acts to promote further deep convection in the region of maximum positive θ_e anomalies. Our analysis indicates a strong role for the NV in the evolution of the AEW and the associated convection. A recent study by Taylor et al. (2004, manuscript submitted to *Quart. J. Roy. Meteor. Soc.*) has also highlighted

the presence of synoptic-scale, westward propagating surface temperature anomalies on the southern fringe of the Sahara. Despite being a integral part of AEW structure (cf. Carlson 1969a,b; Thorncroft and Hodges 2001), the NVs have received little attention in the literature given to these features. Given their prominence and their potential impact on convection, more analysis of these key features is required.

It can be observed from the maps in the previous sections that west of the Greenwich meridian the low-level θ perturbation (and associated NV) moves to the west-northwest (approximately following the mean low-level θ gradient (Fig. 3c), whereas the PV perturbation (and embedded maxima) moves westward in the direction of the mean AEJ (Fig. 3a). These structural changes imply that the amount of growth via a baroclinic mechanism reduces with time. However, the interactions between the PV maxima embedded within the AEJ-level PV perturbation and PV maxima generated by convection over the Guinea highlands are key for the next phase of the AEW life cycle.

c. *Phase (iii): West coast developments*

The third phase of the AEW life cycle preceding tropical cyclogenesis is shown schematically in Fig. 10c. At this stage, the system loses much of its baroclinic character, with the perturbation to the low-level θ gradient becoming severely distorted near the West African coast and the midtropospheric PV maxima dominating the signal of this system. The westward propagating PV maxima within the perturbation to the PV strip move closer to the stationary PV maxima over the Guinea highlands and they begin to interact. Near the coast these regions of PV maxima merge and convection continues to occur. This results in a deep, moist [ECMWF analysis suggests >90% relative humidity from the surface to approximately 300 hPa (not shown)] PV column that has a cyclonic circulation near the surface. Satellite observations (Fig. 4) show that soon after this PV column leaves the West African coast convection becomes more organized and a cyclonic circulation is able to reach the ocean surface [diagnosed by quick scatterometer (QuikSCAT) surface wind observations (not shown)]. This signifies the onset of tropical cyclogenesis.

We argue that tropical cyclogenesis does not result directly from the synoptic-scale AEW, but rather from the merger of embedded mesoscale vortices that amplify over the continent in the AEW structure. This is consistent with Montgomery and Enagonio (1998) who simulated the merger of subsynoptic-scale PV anomalies and the effects of penetrative convection on a midlevel vortex, showing that the axisymmetrization process resulted in the development of a surface cyclone. Simpson et al. (1997) looked at some examples of tropical cyclogenesis resulting from the interactions between mesovortices in the western Pacific, showing structures that are qualitatively similar to those seen leaving the West African coast in this case.

The Guinea highlands were noted by Erickson (1963) as the origin of a subsynoptic-scale surface vortex that was the precursor to Hurricane Debbie (1961) (which also formed very close to the African coast). These highlands are also highlighted by the tracking statistics of Thorncroft and Hodges (2001) that show this region is a genesis site of 850-hPa vorticity centers. The results of these previous studies and this case study imply that the processes that occur over the Guinea highlands have important repercussions on downstream development and require further investigation.

6. Summary and final comments

We have presented an analysis of the evolution of an AEW, from initiation over the African continent until leaving the West African coast using ECMWF operational analysis, satellite imagery, and synoptic observations. The results shown have promoted the division of this life cycle into three distinct phases: this AEW develops near 20°W, in response to a large convective event that occurs over the Darfur region of Sudan [phase (i)]. This is followed by a period of baroclinic development over West Africa, which is reinforced by diabatically generated subsynoptic-scale PV maxima [phase (ii)]. These PV maxima merge with one another and with PV maxima generated over the Guinea highlands and result in a strong vortex leaving the West African coast [phase (iii)]. A short time later this vortex is responsible for the genesis of a tropical cyclone.

In this study, particular emphasis was placed on a PV–θ analysis, which highlights both the synoptic wavelike structure at the same time as embedded subsynoptic-scale diabatically generated PV anomalies. This approach also highlighted the role of a significant low-level circulation center on the southern fringe of the Sahara, which formed part of the baroclinic structure. We argue that this feature was also able to influence the nature of the convection via advection of low-level θ_e.

Greatest uncertainties occur when examining the subsynoptic-scale features, such as the diabatically generated PV anomalies, which we have shown are an important part of the scale interactions. This occurs primarily because routine observations are sparse across the whole of tropical North Africa. These uncertainties can only be addressed by using either high-resolution numerical models or a vastly improved observation network in West Africa. Observations of the quality required can only realistically be achieved through a special observing campaign, such as the proposed African Monsoon Multidisciplinary Analyses (AMMA) project (see AMMA Web site for more details: http://www.joss.ucar.edu/amma).

The similarity of the structures seen in this case to those shown in composite studies tentatively suggests

that this type of evolution is common, but more research is required. Future work will include more in-depth case studies to determine if the features and processes highlighted in this study are common in all AEWs, what the key differences are between intense and weak events, and what the consequences are for downstream tropical cyclones.

Acknowledgments. The ECMWF operational analyses were obtained from the National Center for Atmospheric Research (NCAR), Meteosat imagery was provided by EUMETSAT, station data came from the British Atmospheric Data Centre (BADC), and QuikSCAT data was provided by the Air–Sea Interaction and Climate Team at the NASA Jet Propulsion Laboratory. We extend our gratitude to Anantha Aiyyer, Dave Vollaro, Doug Parker, Ron McTaggart-Cowan, and John Molinari for their help and discussions during this research. We would also like to thank Kay Shelton, Karen Mohr, and two anonymous reviewers for useful discussion and comments that helped to improve the manuscript. This work has been funded by NSF (PTAEO: 1023911-1-24796).

REFERENCES

Albignat, J. P., and R. J. Reed, 1980: The origin of African wave disturbances during phase III of GATE. *Mon. Wea. Rev.,* **108,** 1827–1839.

Avila, L. A., and R. J. Pasch, 1992: Atlantic tropical systems of 1991. *Mon. Wea. Rev.,* **120,** 2688–2696.

Bevan, J., cited 2000: Tropical cyclone report, Hurricane Alberto 3–23rd August 2000. National Hurricane Center, Miami, FL. [Available online at http://www.nhc.noaa.gov/2000alberto.html.]

Burpee, R. W., 1972: The origin and structure of easterly waves in the lower troposphere of North Africa. *J. Atmos. Sci.,* **29,** 77–90.

——, 1974: Characteristics of North African easterly waves during the summers of 1968 and 1969. *J. Atmos. Sci.,* **31,** 1556–1570.

Carlson, T. N., 1969a: Synoptic histories of three African disturbances that developed into Atlantic hurricanes. *Mon. Wea. Rev.,* **97,** 256–276.

——, 1969b: Some remarks on African disturbances and their progress over the tropical Atlantic. *Mon. Wea. Rev.,* **97,** 716–726.

Charney, J. G., and M. E. Stern, 1962: On the stability of internal baroclinic jets in a rotating atmosphere. *J. Atmos. Sci.,* **19,** 159–172.

Dickinson, M., and J. Molinari, 2000: Climatology of sign reversals of the meridional potential vorticity gradient over Africa and Australia. *Mon. Wea. Rev.,* **128,** 3890–3900.

Duvel, J. P., 1990: Convection over tropical Africa and the Atlantic Ocean during northern summer. Part II: Modulation by easterly waves. *Mon. Wea. Rev.,* **118,** 1855–1868.

Erickson, C. O., 1963: An incipient hurricane near the West African coast. *Mon. Wea. Rev.,* **91,** 61–68.

Fink, A. H., and A. Reiner, 2003: Spatio-temporal variability of the relation between African easterly waves and West African squall lines in 1998 and 1999. *J. Geophys. Res.,* **108,** 4332, doi:10.1029/2002JD002816.

Frank, N. L., 1970: Atlantic tropical systems of 1969. *Mon. Wea. Rev.,* **98,** 307–314.

Hertenstein, R. F. A., and W. H. Schubert, 1991: Potential vorticity anomalies associated with squall lines. *Mon. Wea. Rev.,* **119,** 1663–1672.

Hill, C. M., and Y.-L. Lin, 2003: Initiation of a mesoscale convective complex over the Ethiopian highlands preceding the genesis of Hurricane Alberto (2000): A precursor to tropical cyclogenesis. *Geophys. Res. Lett.,* **30,** 1232, doi:10.1029/2002GL016655.

Hodges, K. I., and C. D. Thorncroft, 1997: Distribution and statistics of African mesoscale convective weather systems based on the ISCCP Meteosat imagery. *Mon. Wea. Rev.,* **125,** 2821–2837.

Hoskins, B. J., M. E. McIntyre, and A. W. Robertson, 1985: On the use and significance of isentropic potential vorticity maps. *Quart. J. Roy. Meteor. Soc.,* **111,** 877–946.

Houze, R. A., Jr., 1989: Observed structure of mesoscale convective systems and implications for large-scale heating. *Quart. J. Roy. Meteor. Soc.,* **115,** 425–461.

Mapes, B. E., 1998: The large-scale part of tropical mesoscale convective system circulations: A linear vertical spectral band model. *J. Meteor. Soc. Japan,* **76,** 29–55.

Montgomery, M. T., and J. Enagonio, 1998: Tropical cyclogenesis via convectively forced vortex Rossby waves in a three-dimensional quasigeostrophic model. *J. Atmos. Sci.,* **55,** 3176–3207.

Parker, D. J., and A. J. Thorpe, 1995: Conditional convective heating in a baroclinic atmosphere: A model of convective frontogenesis. *J. Atmos. Sci.,* **52,** 1699–1711.

Payne, S. W., and M. M. McGarry, 1977: The relationship of satellite inferred convective activity to easterly waves over West Africa and the adjacent ocean during phase III of GATE. *Mon. Wea. Rev.,* **105,** 413–420.

Pytharoulis, I., and C. D. Thorncroft, 1999: The low-level structure of African easterly waves in 1995. *Mon. Wea. Rev.,* **127,** 2266–2280.

Raymond, D. J., and H. Jiang, 1990: A theory for long-lived mesoscale convective systems. *J. Atmos. Sci.,* **47,** 3067–3077.

Reed, R. J., D. C. Norquist, and E. E. Recker, 1977: The structure and properties of African wave disturbances as observed during phase III of GATE. *Mon. Wea. Rev.,* **105,** 317–333.

Simmons, A. J., and B. J. Hoskins, 1979: The downstream and upstream development of unstable baroclinic waves. *J. Atmos. Sci.,* **36,** 1239–1254.

Simpson, J., E. Ritchie, G. J. Holland, J. Halverson, and S. Stewart, 1997: Mesoscale interactions in tropical cyclone genesis. *Mon. Wea. Rev.,* **125,** 2643–2661.

Thorncroft, C. D., and B. J. Hoskins, 1994a: An idealized study of African easterly waves. Part I: A linear view. *Quart. J. Roy. Meteor. Soc.,* **120,** 953–982.

——, and ——, 1994b: An idealized study of African easterly waves. Part II: A non linear view. *Quart. J. Roy. Meteor. Soc.,* **120,** 983–1015.

——, and M. Haile, 1995: The mean dynamical and thermodynamic fields for July 1989 over tropical North Africa and their relationship to convective storm activity. *Mon. Wea. Rev.,* **123,** 3016–3031.

——, and M. Blackburn, 1999: Maintenance of the African easterly jet. *Quart. J. Roy. Meteor. Soc.,* **125,** 763–786.

——, and K. Hodges, 2001: African easterly wave variability and its relationship to Atlantic tropical cyclone activity. *J. Climate,* **14,** 1166–1179.

Williams, E., and N. Renno, 1993: An analysis of the conditional instability of the tropical atmosphere. *Mon. Wea. Rev.,* **121,** 21–36.